Eur. Phys. J. B **37**, 473–478 (2004)
DOI: 10.1140/epjb/e2004-00083-3

THE EUROPEAN PHYSICAL JOURNAL B

Effects of topological defects in the semiconductor carbon nanotube intramolecular junctions

W. Fa[1,2,a], J. Chen[1], and J. Dong[1]

[1] National Laboratory of Solid State Microstructures and Department of Physics, Nanjing University, Nanjing 210093, P.R. China
[2] Department of Applied Physics, Nanjing University of Aeronautics and Astronautics, Nanjing 210016, P.R. China

Received 29 November 2003
Published online 9 April 2004 –

Abstract. Several intramolecular junctions (IMJs) connecting two semiconductor single-wall carbon nanotubes (SWNTs) have been realized by using the layer-divided technique and introducing the pentagon-heptagon topological defects. The atomic structure of each IMJ is optimized with a combination of density-functional theory (DFT) and the universal force field (UFF) method, based upon which a π-orbital tight-binding calculation is performed on its electronic properties. Obtained results indicate that different topological defects and their distributions on the interfaces of the IMJs have decisive effects on the electronic properties of the IMJs. The specific geometrical defects control the localized defect states chiefly, while the diameters of the SWNTs on both sides are also related to them. The influence on the experimental observation brought by the choice of the scanning line is also presented by comparing the scanning results performed on the defect side with those on the defect-free side. A new IMJ structure has been found, and it probably reflects the real atomic structures of the semiconductor-semiconductor (S-S) IMJ [Phys. Rev. Lett. **90**, 216107 (2003)].

PACS. 61.46.+w Nanoscale materials: clusters, nanoparticles, nanotubes, and nanocrystals – 73.20.At Surface states, band structure, electron density of states – 73.40.Lq Other semiconductor-to-semiconductor contacts, p-n junctions, and heterojunctions

1 Introduction

A single-walled carbon nanotube (SWNT), which is a rolled-up graphite sheet, can be either a semiconductor or a metal, depending on its helicity and diameter [1–4]. This remarkable property suggests that quasi-one-dimension IMJs can be realized by connecting two segments of SWNTs with pentagon-heptagon (5-7) defects [5–10], for which interesting properties may be expected. An intensive effort to understand the physical properties of IMJs is now made due to their promising engineering applications [11–15]. For example, the metal-semiconductor (M-S), metal-metal (M-M) and semiconductor-semiconductor (S-S) IMJs can be used for the building blocks of the quantum nano-electronic and electro-optical devices. Although a great progress in the research of the IMJs has been made, there are still a lot of experimental and theoretical uncertainties about the close relationships between their physical properties and corresponding geometrical structures, especially the effects of the topological defects in the interface region. Since the existing techniques can not detect the 5-7 defects directly, a combination of the experimental observations and the related computational simulations becomes a useful method to study the problems about the IMJs and give further insight of these 'molecular-scale' devices.

It is well-known that non-hexagonal geometrical structures, e.g., pentagons, heptagons, and their different combinations, are required to form the SWNT IMJ and usually called the topological defects, which can scatter electrons and in turn induce the localized states in the interface region. Such localized states were first observed in the (9,6)/(11,8) M-M IMJ [10], and more recently also detected in the (15,2)/(19,3) S-S IMJ by using scanning tunneling microscopy (STM) [16]. However, the (21,−2)/(22,−5) M-S IMJ produced in the experiment was found to have an electronically sharp interface without the localized junction states [10]. Therefore, it is natural to ask whether existence of the localized states in the IMJ reflects a specific configuration of the topological defects. What is the relationship between geometrical and electronic properties of the junction? All of these problems are very important and interesting in the present researches on the SWNT IMJs.

In this paper, we pay more attention to the different possible geometrical structures in the S-S (15,2)/(19,3) IMJ and their effects on its electronic properties. The tight-binding (TB) numerical simulations have been

[a] e-mail: fa_wei@hotmail.com

performed to study the local density of states (LDOSs) and changes of the LDOS caused by the Stone-Wales transformation, showing how these changes can be closely related to the defect structures. To further understand the electronic properties of IMJs, we construct other S-S IMJs with the same defect structure to illustrate the effects of tube diameters. Our results also provide a new reasonable model for the experimentally observed atomic-level junction, which will be helpful to understand clearly the origin of the localized states in the junction region, and reveal details of IMJ physics.

This paper is organized as follows. In Section 2, we briefly introduce the layer-divided technique to construct the different S-S IMJs, followed by geometrical optimizations with a combination of density-functional theory (DFT) and the universal force field (UFF) method. The TB results for the electronic properties of the S-S IMJs are discussed in detail in Section 3. Some concluding remarks are offered in Section 4.

2 Different geometrical structures of the S-S IMJ

The geometrical structure of a SWNT can be uniquely determined by a chiral vector $\vec{C} = n\vec{e}_1 + m\vec{e}_2$, where $\vec{e}_1$ and $\vec{e}_2$ are two primitive lattice vectors of the graphite sheet and (n, m), a pair of integer. On the other hand, we can also divide a chiral (n, m) SWNT into a series of connecting closed "zigzag rings" [17]. Each ring contains n steps along $\vec{e}_1$ and m steps along $\vec{e}_2$, and can be visualized as the "unit cell" of the tube, which consists of $k = 2(n + m)$ connected lattice points, labeled the 1st, 2nd, ..., and Kth, respectively. Therefore, each lattice point on the SWNT surface can be described by another pair of integers (l, k), where l is the ring label and $k = 1, 2, ..., K$ represents the lattice point along the lth ring. Advantage of such a description for a SWNT is to facilitate the formation of various IMJs with a junction region containing only pentagons, hexagons and heptagons.

The first step for constructing an IMJ by addition of topological defects in the hexagonal lattice is to generate a two-dimensional map of the IMJ structure. We put the divided layers of two different SWNT segments in a plane, making them close to each other as possible as they can. The convolution from this map to the three-dimensional tubular structure can be made by a transformation into the cylinder coordinate in the same axial direction. Of course, the differences in diameter and helicity between the two SWNTs cause appearance of geometrical defects on the interface of the IMJ under the constraint of each atom having only threefold coordinates. Owing to the Stone-Wales transformation [18], we can change the atomic structure of a junction by rotating a C−C bond around its center to introduce more topological defects and form various connections. The size of an IMJ interface depends on the number and arrangement of the defects in it.

Since this 3-D construction does not provide correct coordinates of atoms, a structural relaxation is followed by the combined density-functional theory (DFT) and the universal force field (UFF) [19,20] method. The optimization processes are carried out on the junction of 6084 atoms, which contains 78 zigzag rings of the (15,2) and (19,3) tube, respectively. The whole junction is firstly relaxed by the UFF with fixed two zigzag rings at both ends. A DFT structural optimization is then applied to a smaller section containing only 299 atoms cut out from the middle part of the junction. The DFT code used here is Accelrys' DMol3 [21], in which the electronic wave functions are expanded in a double-numeric polarized (DNP) basis set with a real-space cutoff of 4.0 Å. Approximation used in the Hamiltonian is the Harris functional [22] with a local exchange-correlation potential [23].

Comparing total energy of different IMJs gives not only the lowest-energy junction from different isomers, but also the information about distribution of the topological defects on the wall. Three different lowest-energy junctions of the (15,2)/(19,3) IMJ are shown in Figure 1. A 90° rotation of a C−C bond denoted by an arrow in Figure 1a can lead to the configuration of Figure 1b, which corresponds to the ground state structure among all configurations with three pentagons and three heptagons connected together and aligned along the tube axis. Although more additive defects will increase the total energy of the junction, an appropriate distribution of the defects can decrease more the total energy to overcome the perturbation caused by an additive 5-7 defect. For instance, the atoms in Figures 1a and 1c get about 0.6 and 4.2 meV/atom higher energy, respectively, than those in Figure 1b, since all the pair defects tend to parallel the tube axis in the model II of Figure 1b.

3 Electronic properties

Electronic properties of the IMJ are studied by a tight-binding model including the carbon π bonds, in which only nearest-neighbor C−C interactions are considered and the two-center hopping integral $V_{pp\pi}$ is assumed to scale with the bond length r_i as $V_{pp\pi} = V_0(r_0/r_i)^2$ [24]. Here, V_0 and r_0 are the hopping parameter and bond length of the perfect tube, respectively. The hopping parameter is set to -2.75 eV, which has been commonly and successfully used in the TB calculations for the fullerenes and carbon nanotubes. Change of the π-orbital parameter only causes the shift of the peak positions while preserving the validity of the conclusions.

The calculated LDOSs in a narrow energy interval around the Fermi level E_F (zero energy) for the (15,2)/(19,3) IMJs are illustrated in Figure 2. Here, we have averaged the LDOS over each section with length of 5 Å, which is numbered along the common tubule axis and begins from the middle of the interface region. That is to say, the indices (1, 2, 3, ..., 6) following "L" and "R" refer to specific sections in the (15,2) and (19,3) parts away from the interface. Therefore, the LDOS as a function of distance from the interface on either side of the

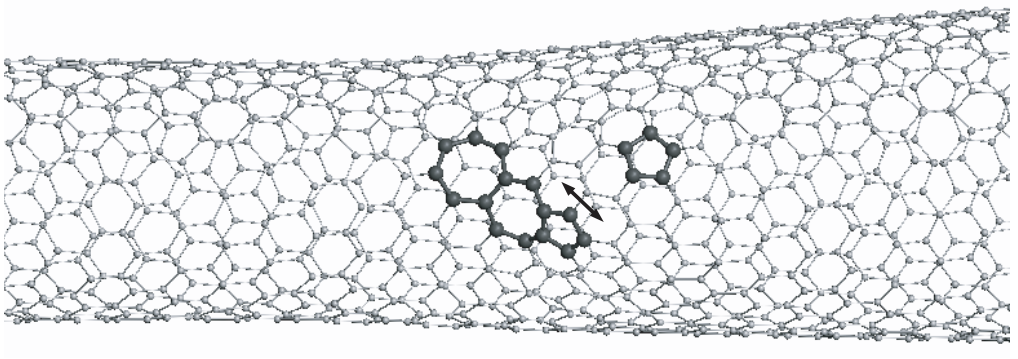

(a) Model I

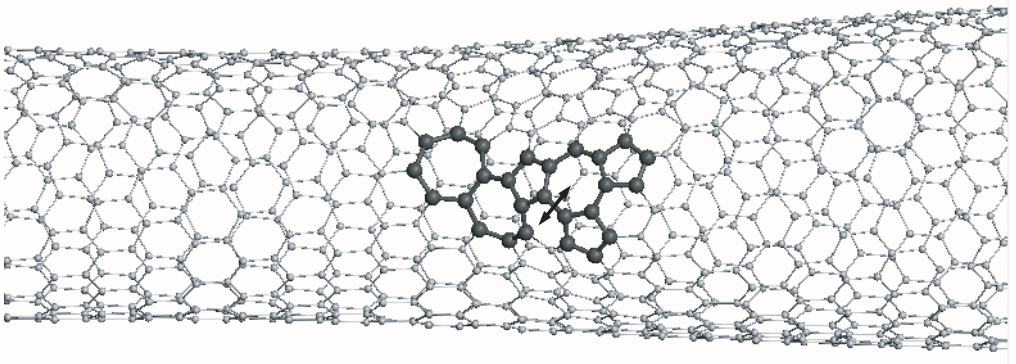

(b) Model II

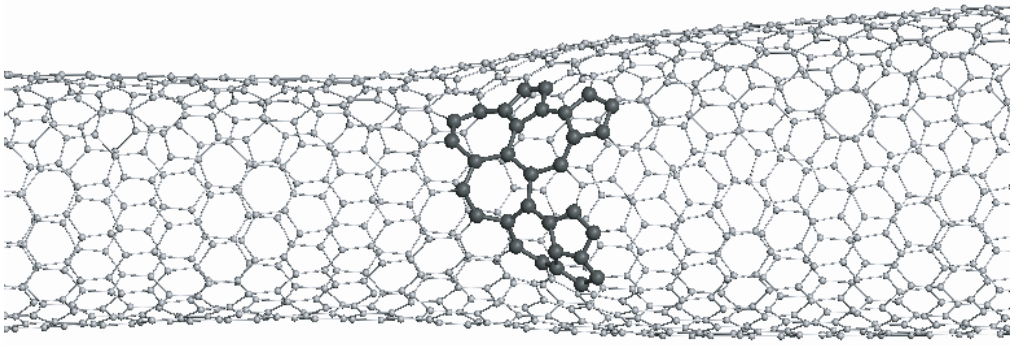

(c) Model III

Fig. 1. Selected several optimized geometrical structures for different defect connections between the (15,2) tube (left) and the (19,3) tube (right), in which carbon atoms of the pentagons and heptagons are indicated by large solid black balls. The models I, II, and III contain a joint section with two, three and four pairs of pentagons and heptagons, respectively.

junction can be directly compared to each other. It is seen clearly from Figure 2 that the LDOSs are mostly distorted in the interface region of L1 and R1, and asymmetric around E_F due to existence of the topological defects. The distortions disappear much more swiftly away from the interface into the (15,2) side than into the (19,3) segment, which reflects the different screening characteristics of the two segments. Far from the interface region, the DOSs of the perfect tubes are progressively recovered. For example, the LDOS curves at L6 and R6 show the basic electronic structures (especially the band gap) of the individual (15,2) and (19,3) tubes, respectively. Such basic features are very similar to those of M-M IMJs [10], except that the spatial decay of the distortion due to the defects lasts 2 nm towards the thinner side and even 3 nm to the thicker side, which is much longer than that of M-M IMJs (only about 1 nm). We think that such a longer decay length makes the S-S IMJ more suitable for studying the effects of the topological defects on the electronic properties, especially for detecting the localized defect state.

Of special interest in the electronic structures of the S-S IMJs is emergence of the localized defect states in the band gap, marked by the broken vertical lines in Figure 2, which are important for designing active devices.

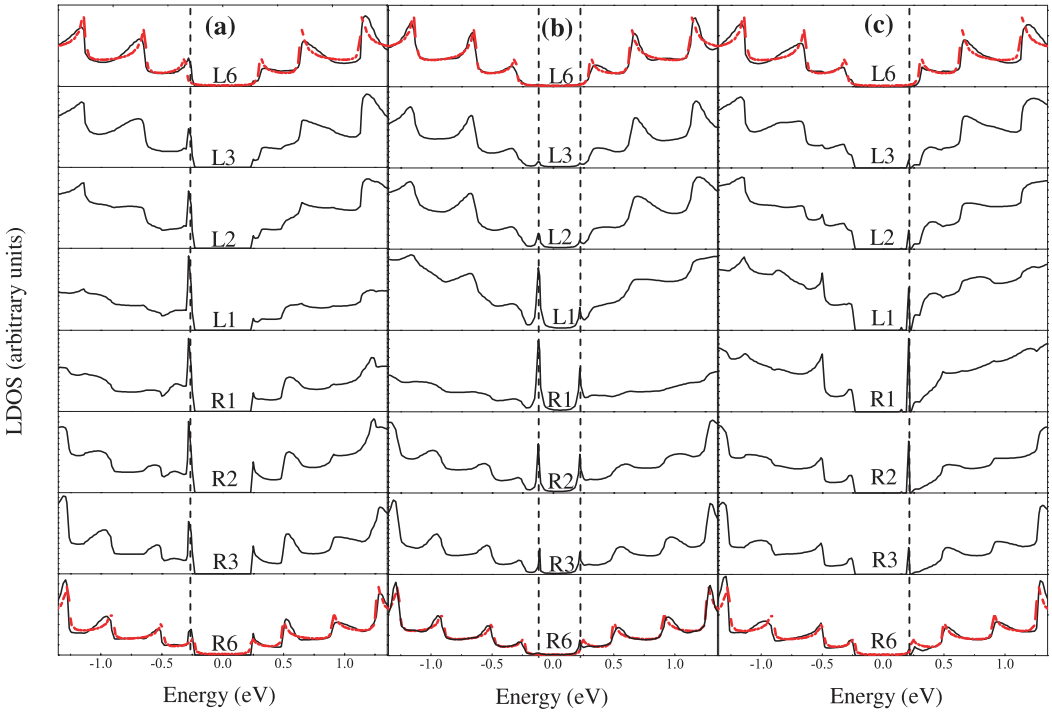

Fig. 2. Calculated LDOS for the models shown in Figure 1, which are averaged over a section with its length of 5 Å. The broken vertical lines indicate the positions of the localized defect states in the interface region. The dashed curves in the top and bottom of the figures correspond to the calculated bulk DOS of the (15,2) and (19,3) tube, respectively.

Obviously, different distributions of the topological defects on the tube wall will cause the diversity of electronic properties at the interface. For example, when we introduce an additional 5/7 defect into the mode I by rotating a bond denoted by an arrow in Figure 1a around its center, the model II is obtained. However, such a small structural difference brings a substantial change of the LDOS at the interface: the localized state resonating with the valence band edge of (19,3) tube in the model I evolves into a pair of the localized defect states in the model II, i.e., one is in the band gap and the other resonates with the conduction band edge of (19,3) tube.

Another interesting point is that the van Hove singularity (VHS) peaks on either side can penetrate into the interface region, particularly for those of IMJs connecting the narrow-gap semiconductor SWNTs. This phenomenon is usually much more obvious for the band edge less perturbed by the defects. For example, the model I has a localized state positioned in the valence band, while penetration of the VHS peak is clearly done in the conduction band of the model I. By investigating various possible defect structures connecting (15,2) and (19,3) tubes, we find the model III shows more similar electronic characteristics to those observed in the experiment [16], in which a localized defect state emerges at 0.21 eV and the first and second VHS peak in the valence band of the (19,3) segment penetrate into the (15,2) segment. We should also mention that the defect state in the model III is closer to the conduction band edge of the right-tube than the experimental observation, which suggests that probably more theoretical and experimental efforts are needed to seek the best matching model among those with as less defects as possible.

We are also concerned with the choice of the scanning line, which may lie at the side with defects or at the defect-free side of an IMJ in the STM experiment, which has definite influences on the scanning tunneling spectroscopy (STS) data. The STS simulations of the model III are given in Figure 3 for these two cases, from which the asymmetry around the defect center is clearly seen in every case. The LDOS oscillations due to perturbation induced by the topological defects, are clearly visible in both cases for the scan results just at the localized defect state of 0.21 eV in the band gap. However, the amplitude and the decay of LDOS are quite different in the two cases. For example, it decays much more gently and slowly towards either side in the case of scanning on the defect-free side. When scanning is performed at the valence band edges of both tubes, the spatial distributions measured on the defect-free side are almost not perturbed, while those on the defect side are mostly distorted around the structural defects within 1 nm. Such distortion is caused by a potential barrier created by the defects. Our calculated results indicate that a correct choice of the scanning line is helpful to detect easily the localized defect, because changes of LDOS, caused by the presence of defects, can be obviously found at various energy levels if the scanning line lies at the defect side.

Finally, in order to know if the constituent SWNTs in an IMJ have real effects on its electronic structures, we have constructed some other S-S IMJs, shown in Figure 4, which connects two zigzag SWNTs with the same

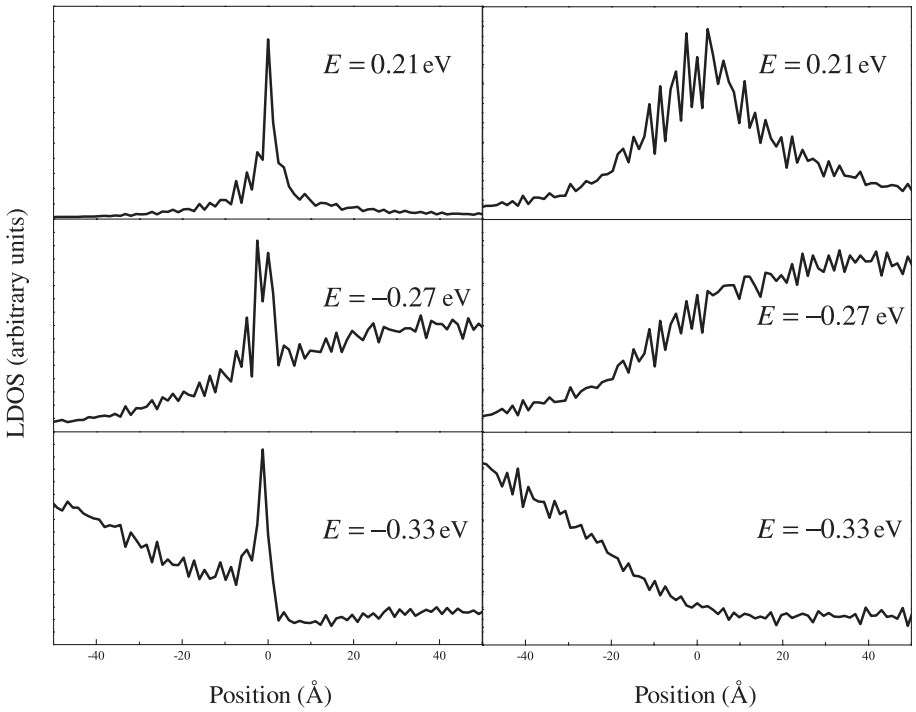

Fig. 3. STS calculation based on the model III, scanned along a line parallel to the junction axis, for three different energy levels. The 0.21 eV matches the localized defect state, while the profiles at −0.27 eV and −0.33 eV show the scan results for the valence band edges of the (19,3) and (15,2) tubes, respectively. The origin represents the defect center, while negative and positive position correspond to the (15,2) and (19,3) tube, respectively. The left and right panels correspond, respectively, to the scanning carried on the defect or defect-free side of the IMJ.

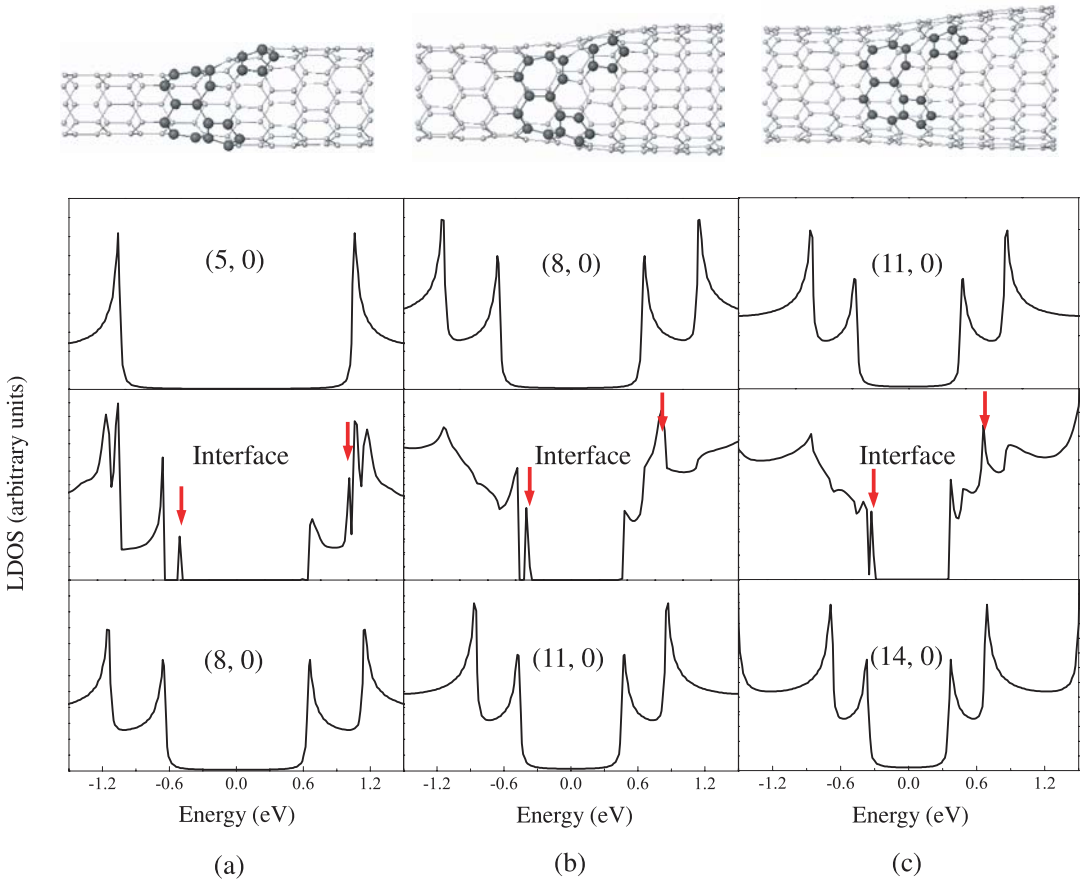

Fig. 4. Calculated π-electron density of states for the (a) (5,0)/(8,0), (b) (8,0)/(10,0) and (c) (11,0)/(14,0) IMJ, whose configurations are shown on the top. The localized defect states coming from the topological defects are indicated by arrows.

diameter ratio of the two constituent tubes as that in the (15,2)/(19,3) IMJ. It is found that the tube diameters can affect the LDOS at the interface of an IMJ in addition to the well-known topological defects at the interface. In particular, we introduce a specific defect configuration to illustrate the effects of tube diameter, which is the same as that in the model I, containing two heptagons plus one pentagon connected together at the concave region and an isolated pentagon at the convex region. Calculated LDOSs are also displayed in Figure 4. The localized defect states, whose positions are determined by the STS simulations, are visible for every IMJ as denoted by arrows in Figure 4. One sharp peak below and above the Fermi level can be ascribed to the topological defects directly, which are distinctly seen from the (5,0)/(8,0) IMJ in Figure 4a. However, the peaks sometimes resonate with the VHS of the tubes on either side, especially for those IMJs with larger diameter tubes since the band gap is inversely proportional to the tube diameter. For example, it is seen from Figure 4b, the localized state in the gap moves close to the valence band edge of the (11,0) tube, while the localized state in the conduction band resonates with the second VHS peaks of the (11,0) tube. Ultimately, in Figure 4c, the localized state in the gap becomes resonant with the first VHS peak in the (11,0)/(14,0) IMJ with further larger diameter tubes. This also explains why the localized states below the Fermi level are not observed in the experiment in which the tubes have larger diameters. In conclusion, we demonstrate that the electronic structure at the interface of the S-S IMJ is decided by the particular distribution of the structural defects and also the diameters of the SWNTs forming the IMJ.

4 Conclusions

We have studied the structural and electronic properties of the S-S IMJs with topological defects. Several kinds of the S-S IMJs are constructed along their common axis firstly by a new layer-divided technique, and then further optimized by the combined DFT-UFF program. Based upon the experimental results, we can determine the most possible geometrical structure among various IMJs. For example, the model III for the (15,2)/(19,3) IMJ probably reflects the real atomic structures of the junction observed in reference [16], since the peak at 0.21 eV obtained by our calculations and other spatially features of the localized states at different energy levels agree with those measured in the experiment.

Our TB calculations indicate that the junctions connecting two semiconducting SWNTs with different diameters can have different electronic properties despite of the similar defect structures. Whether or not the localized states emerge in the band gap is mainly determined by the defect distribution at the surface of the IMJ, which is also affected by the diameters of two tubes on both sides. For the IMJ composed of SWNTs with the larger diameters, the localized states have increasing probability to resonate with the VHS peaks of the SWNT on each side. Additionally, the scanning line on the defect side is helpful to detect the localized defect states. Compared to the shorter decay distance observed in the M-M IMJ, the longer spatial decay of the localized states in the S-S IMJ is much easier to be detected across the junction interface, which will be profitable for further understanding the IMJ at the atomic level.

This work was supported by the Natural Science Foundation of China under Grant No. 10074026. The authors acknowledge also support from a Grant for State Key Program of China through Grant No. 1998061407.

References

1. J.W. Mintmire, B.I. Dunlap, C.T. White, Phys. Rev. Lett. **68**, 631 (1992)
2. N. Hamada, S.I. Sawada, A. Oshiyama, Phys. Rev. Lett. **68**, 1579 (1992)
3. R. Saito, M. Fujita, G. Dresselhaus, M.S. Dresselhaus, Appl. Phys. Lett. **60**, 2204 (1992)
4. T.W. Odom, J.L. Huang, P. Kim, C.M. Lieber, Nature **391**, 62 (1998)
5. L. Chico, V.H. Crespi, L.X. Benedict, S.G. Louie, M.L. Cohen, Phys. Rev. Lett. **76**, 971 (1996)
6. L. Chico, L.X. Benedict, S.G. Louie, M.L. Cohen, Phys. Rev. B **54**, 2600 (1996)
7. J.C. Charlier, T.W. Ebbesen, Ph. Lambin, Phys. Rev. B **53**, 11108 (1996)
8. D. Orlikowski, M.B. Nardelli, J. Bernholc, C. Roland, Phys. Rev. Lett. **83**, 4132 (1999)
9. M.S. Ferreira, T. Dargam, R.B. Muniz, A. Latge, Phys. Rev. B **62**, 16040 (2000)
10. Min Ouyang, Jin-Lin Huang, Chin Li Cheung, C.M. Lieber, Science **291**, 97 (2001)
11. S.J. Tans, A.R.M. Verschueren, C. Dekker, Nature **393**, 49 (1998)
12. R. Martel, T. Schmidt, H.R. Shea, T. Hertel, Ph. Avouris, Appl. Phys. Lett. **73**, 2447 (1998)
13. P.G. Collins, A. Zettl, H. Bando, A. Thess, R.E. Smalley, Science **278** (1999)
14. Z. Yao, H.W.C. Postma, L. Balents, C. Dekker, Nature **402**, 273 (1999)
15. M. Fuhrer, J. Nygard, L. Shih, M. Foreo, Y.-G. Yoon, M.S.C. Mazzoni, H.J. Choi, J. Ihm, S.G. Louie, A. Zettl, P.L. McEuen, Science **288**, 494 (2000)
16. Hajin Kim, J. Lee, S.-J. Kahng, Y.-W. Son, S.B. Lee, C.-K. Lee, J. Ihm, Young Kuk, Phys. Rev. Lett. **90**, 216107 (2003)
17. Huatong Yang, Jinming Dong, Dingyu Xing, Chin. Phys. Lett. **18**, 1105 (2001)
18. A.J. Stone, D.J. Wales, Chem. Phys. Lett. **128**, 501 (1986)
19. A.K. Rappe, C.J. Casewit, K.S. Colwell, W.A. Goddard, W.M. Skiff, J. Am. Chem. Soc. **114**, 10024 (1992)
20. N. Yao V. Lordi, J. Appl. Phys. **84**, 1939 (1998)
21. B. Delley, J. Chem. Phys. **92**, 508 (1990); B. Delley, J. Phys. Chem. **100**, 6107 (1996); `http://www.accelrys.com/mstudio/dmol3.html`
22. J. Harris, Phys. Rev. B **31**, 1770 (1985)
23. S.H. Vosko, L. Wilk, M. Nusair, Can. J. Phys. **58**, 1200 (1980)
24. W.A. Harrison, *Electronic Structure and the Properties of Solids* (Dover, New York, 1989)